SLAC–PUB–4821
DPNU-88-50
February 1989
(T/E)

RECENT RESULTS ON $S = -3$ BARYON SPECTROSCOPY FROM THE LASS SPECTROMETER*

D. ASTON,[1] N. AWAJI,[2a] T. BIENZ,[1] F. BIRD,[1] J. D'AMORE,[3]
W. DUNWOODIE,[1] R. ENDORF,[3] K. FUJII,[2b] H. HAYASHII,[2c] S. IWATA,[2b]
W.B. JOHNSON,[1] R. KAJIKAWA,[2] P. KUNZ,[1] D.W.G.S. LEITH,[1] L. LEVINSON,[1d]
T. MATSUI,[2b] B.T. MEADOWS,[3] A. MIYAMOTO,[2b] M. NUSSBAUM,[3] H. OZAKI,[2]
C.O. PAK,[2b] B.N. RATCLIFF,[1] D. SCHULTZ,[1] S. SHAPIRO,[1] T. SHIMOMURA,[2e]
P. K. SINERVO,[1f] A. SUGIYAMA,[2] S. SUZUKI,[2] G. TARNOPOLSKY,[1g]
T. TAUCHI,[2b] N. TOGE,[1] K. UKAI,[4] A. WAITE,[1h] S. WILLIAMS[1]

[1] *Stanford Linear Accelerator Center, Stanford University, Stanford, CA 94309*
[2] *Department of Physics, Nagoya University, Furo-cho, Chikusa-ku, Nagoya, Japan*
[3] *University of Cincinnati, Cincinnati, OH 45221*
[4] *Institute for Nuclear Study, University of Tokyo, Midori-cho, Tanashi, Tokyo, Japan*

Invited talk by B.T. MEADOWS
Presented at the SLAC 16th Summer Institute on Elementary Particle Physics,
Stanford, California, July 17–28, 1988.

---

* Work supported in part by the Department of Energy under contract No. DE–AC03–76SF00515; the National Science Foundation under grant Nos. PHY82–09144, PHY85–13808, and the Japan U.S. Cooperative Research Project on High Energy Physics.

Present Addresses :

a Fujitsu Limited, Nakahara-ku, Kawasaki 211, Japan.
b National Laboratory for High Energy Physics, KEK, Oho-machi, Tsukuba, Ibaraki 305, Japan.
c Nara Women's University, Kitauoya-nishi-machi, Nara-shi, Nara 630, Japan.
d Weizmann Institute, Rehovot 76100, Israel.
e Nippon BIO-RAD Laboratories, 1-2-7 Shiba-Daimon, Minato-ku, Tokyo 105, Japan.
f University of Pennsylvania, Philadelphia, Pennsylvania 19104, U.S.A.
g Hewlett-Packard Laboratories, 1501 Page Mill Road, Palo Alto, California 94304, U.S.A.
h Department of Physics, University of Victoria, Victoria BC, Canada V8W 2Y2

ABSTRACT

Data demonstrating the existence of two Ω^{*-} resonances produced in K^-p interactions at 11 GeV/c in the LASS spectrometer are presented. The first state is seen in the $\Xi^{*o}K^-$ decay channel with mass 2253 ± 13 MeV/c^2 and width 81 ± 38 MeV/c^2, and the second in the $\Omega^-\pi^+\pi^-$ system with mass 2474 ± 12 and width 72 ± 33 MeV/c^2. Inclusive cross sections corresponding to these decays corrected for unseen charge modes are estimated to be respectively 630 ± 180 and 290 ± 90 nb, respectively.

1. INTRODUCTION

Even though the Ω^- hyperon was discovered more than two decades ago, data showing the existence of any of its excited states have become available only very recently.[1-3] Such data have required the use of K^- or hyperon beams in fixed target experiments. They also require detectors with the acceptance and resolution necessary to deal efficiently with the complex topologies that events involving such particles entail, the capability to perform good particle identification necessary in the recognition of the relevant final states, and the ability to acquire and process huge data samples. These qualities have been admirably matched by the Large Aperture Superconducting Solenoid (LASS) spectrometer at SLAC. In this paper, we present the data which were accumulated in a large exposure of the LASS spectrometer to a beam of 11 GeV/cK^-. These data clearly demonstrate the existence of Ω^{*-} resonances in two channels:

$$K^-p \to \underbrace{\Xi^-}_{\hookrightarrow \Lambda\pi^-}\pi^+K^- + \text{anything} \quad ; \tag{1}$$

$$K^-p \to \underbrace{\Omega^-}_{\hookrightarrow \Lambda K^-}\pi^+\pi^- + \text{anything} \quad . \tag{2}$$

2. THE EXPERIMENT

The LASS spectrometer is shown in Fig. 1. Full descriptions of the hardware, triggering and data processing algorithms and other experimental details are given in Ref. 4. Details associated with extraction of the Ξ^- and Ω^- samples discussed here are also given in Ref. 5.

The spectrometer was situated in an RF-separated beam of 11 GeV/c K^- with a K/π ratio of 70/1, tagged by beam Čherenkov counters. Important features of LASS were its uniform acceptance over almost the full 4π solid angle, excellent momentum and angular resolution, azimuthal symmetry, and good particle identification. Momentum measurement was accomplished with the superconducting solenoid with 22.4 kG field in the beam direction, and with the 30 kG-m dipole with vertical field. Low momentum particles were well-measured by the solenoid vertex detector which was instrumented with proportional wire chambers (PWC's) having 200 μm spatial resolution. High momentum particles travelling close to the beam axis were accurately measured in the dipole spectrometer.

Particle identification was accomplished by two threshold Čherenkov counters (C_1 and C_2) and a time of flight (TOF) hodoscope placed behind C_1 at a distance of five meters downstream from the target. The pulse heights measured in the cylindrical PWC's surrounding the target provided dE/dx information for low momentum particles having wide recoil angles. This was useful in distinguishing $\pi/K/p$ hypotheses in the $1/\beta^2$ region.

A very loose trigger required two or more charged particles to emerge from the hydrogen target. For the channels of interest here this represented a completely negligible bias.

The raw data sample contained $\sim$ 113 million triggers, and the resulting useful K^- beam flux corresponded to a sensitivity of 4.1 events/nb. After track reconstruction, a sample of events consistent with the $\Xi^- \rightarrow \Lambda\pi^-$ or $\Omega^- \rightarrow \Lambda K^-$ decay topologies, illustrated in Fig. 2, was identified. A pair of oppositely-charged tracks which met within a few mm in space was required to yield a $p\pi^-$ effective mass consistent with the nominal Λ mass. The Λ momentum vector was further required to point back within a few mm of a negative track candidate which was chosen such that the effective mass formed with the Λ was compatible with either of the above decay modes.

Finally, the composite track formed from this negative with the Λ was, in turn, required to extrapolate back to within 1 cm of a primary vertex, whose position was determined by a fit to the incoming beam and the primary charged-track candidates. A sample of $\sim$ 1.5 million events satisfying these requirements was defined.

3. THE $\Xi^- K^- \pi^+$ CHANNEL

A clean sample of Ξ^- events was readily extracted. Particle identification was used to reject events inconsistent with a Ξ^- interpretation, and also events with identified protons at the primary vertex. Kinematic overlap between γ and Λ often occurred. Such misidentified γ's were removed from the remaining Λ sample by eliminating events with Λ decay helicity cosine greater than 0.98. Finally, only events with a Ξ^- track length greater than 3 cm were retained. The resulting $\Lambda\pi^-$ effective mass distribution shown in Fig. 3 exhibited a strong Ξ^- signal. Approximately 82,000 Ξ^- events with a background of approximately 10% in the mass range $1310 < M_{\Lambda\pi^-} < 1332$ MeV/c^2 were selected for further study.

These events were then tested for existence of a K^-. Clearly, a negative track produced in K^-p induced Ξ^- reactions was more likely to be a π^- than a K$^-$, since the latter required production of an additional unit of strangeness. Clear identification of the K^- was therefore necessary, and to this end negative tracks entering the geometrically efficient regions of C_1 or C_2 at momenta above 2.9 GeV/c were required to give no light. To reduce background from poorly measured π^-'s below threshold, K^- candidates were also required to have momenta at least two standard deviations above threshold.

Since K^- identification required a negative signature (no light) from the Čherenkov counters, it was essential to obtain an accurate estimate of the "punch through" contamination in the K^- sample produced by π^-'s (or e^-'s) failing to produce light due to Čherenkov inefficiency. This estimate was derived from the particles which did give Čherenkov light. The momentum distributions for negative particles from primary vertices of events in the Ξ^- sample were examined, and are shown in Fig. 4. These distributions were weighted, on a particle-by-particle basis, by factors depending upon the Čherenkov efficiencies (ϵ), which in turn depended upon the particle momentum and hit position. The points on the dotted curve corresponded to particles which produced light in at least one C, and were weighted by the factor ϵ^{-1}. This distribution was taken to represent the π^- (and e^-) sample. The threshold near 2.6 GeV/c was clearly seen, and events below this were presumed to be due to e^-. Also in Fig. 4 (points on the solid line) was the distribution representing those particles which gave no light in either C_1 or C_2. This was corrected for efficiency by taking the difference between the momentum distribution for all negative particles (whether giving light or not) and the distribution described above. The sharp fall with increasing momentum near threshold arose because the efficiency increased in this region. Above threshold, this could be taken to represent the K^- momentum distribution. The points on the dashed curve resulted from plotting the momenta of the negative particles giving light, weighted by the factor $\epsilon^{-1}(1-\epsilon)$. This curve represented, therefore, the punch-through contamination. Comparing this with the K^- distribution, it was clear that above the 2.9 GeV/c cut, a rather clean K^- sample was separated.

In this way, a sample of 814 events was extracted, yielding 1,259 $\Xi^- K^- \pi^+$ mass combinations shown in the distribution in Fig. 5. No clear resonant structure was seen in this $S = -3$ baryon system. However, the mass distribution for the $\Xi^-\pi^+$ subsystems (Fig. 6) showed a strong $\Xi^{*o}(1530)$ signal. Selection of an enriched $\Xi^{*o}(1530)$ sample ($1510 < M_{\Xi^-\pi^+} < 1555$ MeV/c^2) resulted in the $\Xi^- K^- \pi^+$ mass histogram of Fig. 7. A clear signal ($\sim$ 4 standard deviations) at a mass of approximately 2250 MeV/c^2 was apparent, and could be interpreted to correspond to the decay of an Ω^{*-} to $\Xi^{*o}(1530)K^-$.

An estimate of the behavior of the non-resonant background beneath the Ξ^{*o} peak in Fig. 6 was made using the events in the sideband regions defined by ($M_{\Xi^-\pi^+} < 1510$ or $1555 < M_{\Xi^-\pi^+} < 1600$ MeV/c^2). The $\Xi^- K^- \pi^+$ mass distribution for these events, normalized to the number of events under the $\Xi^{*o}(1530)$

signal was plotted in Fig. 7 with solid dots. The striking absence of any peak near 2250 MeV/c^2 was a clear indication that the observed structure was associated purely with $\Xi^{*o}(1530)$.

In order to investigate the possibility that the effect arose from π^-'s being misidentified as a result of Čherenkov inefficiency, a study was made using events which were selected exactly as above, except that the "K^-" tracks were required to give light in either C_1 or C_2. All momentum requirements were as before, and the tracks were still assigned a K^- mass. The $\Xi^{*o}(1530)$"K^-" mass distribution that resulted (Fig. 8), contrasted with the true K^- distribution, showing no structure suggestive of a peak in the 2250 MeV/c^2 region. In addition to demonstrating that the peak was not due to misidentified pions, this also showed that it was not a kinematic effect due to the acceptance limitations placed upon the negative track by the Čherenkov identification requirement. An estimate of the mass distribution corresponding to punch-through was also obtained from these "K^-" events by plotting them, each weighted by a factor $(1-\epsilon)/\epsilon$ (where ϵ was the π^- Čherenkov efficiency). This distribution, indicated by open dots in Fig. 7, showed that such punch-through contributed negligibly to the signal.

The significance of the Ω^{*-} signal was estimated from the background subtracted $\Xi^{*o}(1530)K^-$ spectrum in Fig. 9. This was obtained from the data of Fig. 7 by subtraction of the Ξ^{*o} sideband distribution (black dots) representing the non-Ξ^{*o} background from the data in the histogram.

The solid curve of Fig. 9 was the result of a fit to the data using the expression:

$$\frac{dN}{dM} = q\left[\frac{c_1}{\left(M_0^2 - M^2\right)^2 + M_0^2\Gamma^2} + c_2 + c_3 M\right]$$

$$\text{with} \quad \Gamma = \Gamma_0\left(\frac{q}{M}\right)\left(\frac{M_0}{q_0}\right) \quad ,$$

where M_0 and Γ_0 were the Ω^{*-} mass and width, respectively; q (q_0) was the K^- momentum in the rest frame of a $\Xi^* K^-$ system of mass $M(M_0)$; and the c_i were fit parameters. The fit, which resulted in a χ^2 of 8.5 for nine degrees of freedom, yielded Ω^{*-} parameter values:

$$\begin{aligned} M_0 &= 2253 \ \pm 13 \quad \mathrm{MeV/c^2} \\ \Gamma_0 &= 81 \quad \pm 38 \quad \mathrm{MeV/c^2} \end{aligned} ,$$

and a corresponding signal of 41.2 ± 10.2 events (~ 4.1 standard deviations). The dotted curve represented the non-resonant background, and appeared to agree well in magnitude and shape with the corresponding π^- punch-through distribution.

4. THE $\Omega^-\pi^+\pi^-$ CHANNEL

The inclusive production cross section of Ω^- was only $\sim 3\%$ of that for Ξ^- [6] and the decay length was approximately three times smaller. These facts made the separation of the Ω^- events in reaction (2) somewhat less straightforward than the selection of the Ξ^- sample discussed above. All events considered as Ω^- candidates were therefore processed through a fitting procedure which was designed to achieve the improvement in resolution of vertex positions necessary to distinguish between those relatively rare events with genuine Ω^- topologies and the more plentiful ones in which the Λ originated directly from the nearby primary vertex. In this procedure, measured coordinates for an event were matched to an Ω^- topological template in which constraints in 3-momentum conservation at each decay vertex and in Λ mass were built in. The χ^2 quality of this fit, and the information it provided on both the Ω^- track length and its uncertainty were required to match criteria which, when added to a set of requirements similar to those used to define the Ξ^- sample, made it possible to identify a clean Ω^- signal which was seen in the ΛK^- mass plot of Fig. 10. A total of about 600 Ω^- were in the peak. In all, approximately 350 Ω^- events, each with at least one $\pm$ charged track combination, were seen above $\sim 9\%$ background within $\pm$ 10 MeV/c^2 of the Ω^- mass, and were considered as candidates for reaction (2).

The $\Omega^-\pi^+\pi^-$ effective mass distribution, shown in Fig. 11(a), showed evidence for a strong signal at $\sim$ 2470 MeV/c^2. In making this plot, all combinations of $\pm$ track pairs were included, as long as they were not inconsistent with a pion identity with respect to the various particle identification devices. An estimate of the background under this peak was obtained from the wrong sign combinations $\Omega^-\pi^\pm\pi^\pm$. These were plotted in Fig. 11(a) normalized to the sample outside the peak region by a linear mass factor and indicate that the peak was more than five standard deviations above this background.

An obvious problem in these events was that, because of strangeness conservation, the existence of the Ω^- implied that the positive track was likely to be a K^+. The strong possibility existed, therefore, that the peak could be due to production of a Ξ^{*-} decaying to $\Omega^- K^+\pi^-$. To investigate this possibility, the combinations in Fig. 11(a) were also plotted with a K^+ mass assigned to the positive track. This $\Omega^- K^+\pi^-$ mass distribution, shown in Fig. 11(b), had no evidence for a peak, indicating that the Ξ^{*-} interpretation was not correct. Other mass hypotheses such as $\Omega^- e^+ e^-, \Omega^- K^+ K^-$ were also studied, and failed to show any significant peak structure, further suggesting that the signal was due to $\Omega^-\pi^+\pi^-$ combinations.

In order to establish that the peak at 2470 MeV/c^2 corresponded to an $S = -3$ baryon system, it was essential to associate it with those events in which some evidence of the identity of the π^+ existed. The dotted distribution in Fig. 11(a) contained events for which Čherenkov identification of π^+ was possible and showed clearly that such information was of rather limited use. This contrasted with the $\Omega^{*-}(2250)$ situation in which the Čherenkov counters gave important information on an event-by-event basis of K^- identification. It was found, however, that for a significant number of positive particles in reaction (2), information from either the dE/dx or time-of-flight (TOF) devices was available, and some K/π separation was possible. The momentum spectra of these particles was such that though discrimination between K and π interpretations for individual events was possible in only a few cases, a statistical analysis did provide effective distinction.

Clean samples of $K^\pm$ and $\pi^\pm$ were selected with which to study the behaviour of both dE/dx and TOF devices at various momenta. In Fig. 12, the ΛK^- mass distribution from the tightly constrained reaction

$$K^- p \rightarrow \quad \Lambda K^- K^+ \qquad (3)$$

observed in the present experiment showed a strong signal demonstrating that baryon exchange production of $\Xi^{*-}(1830)$ was present. These events were chosen to provide a small, but very clean, sample of K^-'s with TOF measurement [Fig. 13(a)], and a somewhat larger, high purity sample of K^+'s having dE/dx information [Fig. 13(d)].

In Fig. 13(a), the difference (in standard deviations) between the TOF calculated under the kaon mass assumption, t^K_{calc}, and the measured value, t_{meas}, was plotted as abscissa, with K^- momentum as ordinate. The plot showed a vertical band of points localized within $\sim \pm 2\sigma$ of the origin, as would be expected for a pure K^- sample. In Fig. 13(d), the abscissa was the natural logarithm of the kaon to pion probability ratio, P_K/P_π, as derived from the induced cathode pulse height signals in the cylindrical PWC's [4]. In this plot, for momenta less than $\sim$0.4 GeV/c, the kaon interpretation was clearly preferred; at higher momenta, the distribution was a vertical band centered at the origin.

Figures 13(b) and (e) were similar TOF and dE/dx plots, respectively, for negative primaries from our Ω^- sample. These particles were almost certain to be π^-, with a very small contamination from e^-. There was virtually no chance they were either K^- or $\overline{p}$. The distribution of Fig. 13(b) was confined almost entirely to the region of positive abscissa, in contrast to that observed in Fig. 13(a). Furthermore, when the expected TOF was re-calculated using the pion mass, the distribution became a narrow, vertical band centered at the origin, demonstrating that these negative tracks were almost entirely π^-'s, as expected. The dE/dx data in Fig. 13(e) for these particles also contrasted with the K^+ population of Fig. 13(b), and showed a clear bias towards negative abscissa at all momenta, as expected for π^-.

The plots for the positive primary particles from the Ω^- sample, shown for TOF and dE/dx data, respectively, in Figs. 13(c) and (f), could clearly be described by a superposition of the two sets of plots discussed above. This agreed exactly with what would be expected for an admixture of both K^+ and π^+. The required separation of the π^+ population could, however, be accomplished in each case.

It was clear from Figs. 13(a) and (b) that the sample having positive abscissa in Fig. 13(c) should contain almost all of the π^+'s together with approximately half the K^+'s, whereas that with negative abscissa should also contain approximately half the K^+'s but only a small fraction of the π^+'s. In Fig. 14(a), the $\Omega^-\pi^+\pi^-$ masses were plotted separately for combinations containing π^+'s from the above two samples. The solid histogram corresponded to those $\Omega^-\pi^+\pi^-$ combinations for which the positive track was predominantly π^+, and indicated a signal similar in position, shape and significance to that of Fig. 11(a). The dashed histogram, constructed from positive tracks from the left side of Fig. 13(c) showed no evidence of a signal. This showed that the signal was associated with genuine $\pi^+\pi^-$ pairs. Furthermore, in the difference between the solid and dashed histograms of Fig. 14(a), the contribution from misidentified K^+'s should cancel, within statistics, thereby yielding a "net TOF-identified π^+" distribution. This distribution also constituted one contribution to the histogram of Fig. 14(b).

A second contribution to Fig. 14(b) was obtained by following a similar procedure with regard to the dE/dx distributions. It was clear from Figs. 13(d) and (e) that the positive particles in Fig. 13(f) could be split into a sample which was predominantly K^+ in the region with momenta below 0.4 GeV/c and positive abscissae, and the remaining sample which was predominantly made up from π^+. In the latter sample, the K^+ contamination would be distributed approximately symmetrically about the ordinate axis. Subtraction of the distribution of $\Omega^-\pi^+\pi^-$ mass combinations formed with positive tracks in this sample with positive abcsissae from the corresponding distribution with negative abscissae could, therefore be taken to represent the "net π^+" distribution. This was found to contain a signal with 10 more events in the 2470 MeV/c^2 region, and was added into Fig. 14(b) giving an aggregate signal which contained approximately 60% of that in Fig. 11(a). The remaining 40% of the signal came from combinations in which the positive track missed both the TOF and dE/dx systems. No combinations were found in which both TOF and dE/dx identification of the π^+ was made.

In addition to establishing the identity of the π^+, the Ω^{*-} hypothesis for the peak in Fig. 11(a) also required that the system had isospin ($I = 0$). This, in turn, required that the $\pi^+\pi^-$ also be in an $I = 0$ state. The effective mass distributions $M_{\pi^+\pi^-}$ in Fig. 15 indicated a broad, structureless form concentrated at low mass values for events in the $\Omega^-\pi^+\pi^-$ peak region [Fig. 15(b)] as well as in the low and high side bands (Figs. 15(a) and 15(c), respectively). In particular, no clear evidence for ρ^0 $(I = 1)$ was seen.

A large Monte Carlo sample of events corresponding to production of an $\Omega^-\pi^+\pi^-$ system in this mass range was generated, with the simulated dipion system in an s−wave. Recoil mass and transverse momentum distributions of the $\Omega^-\pi^+\pi^-$ systems were produced to simulate the data as closely as possible. These events were then subjected to the identical analysis to the data, and curves indicating the dipion mass shapes were drawn, suitably normalised upon the distributions in Fig. 15. This s−wave behaviour clearly described the data well, indicating therefore a predominance of $I = 0$ in the $\Omega^-\pi^+\pi^-$ peak region, and providing further evidence of Ω^{*-} production.

A fit to the $\Omega^-\pi^+\pi^-$ mass distribution in Fig. 11(a), similar to that for the $\Xi^{*o}K^-$ plot, led to a mass of 2474 ± 12 MeV/c^2 and a width of 72 ± 33 MeV/c^2 for this Ω^{*-}. This is shown in Fig. 16. The acceptance of LASS was computed using the Monte Carlo event sample discussed above, and the cross section for inclusive production of $\Omega^{*-}(2470)$ from 11 GeV/c K^-p interactions with decay to $\Omega^-\pi^+\pi^-$ corrected for unseen charge modes was determined to be 290 ± 90 nb. A similar computation was made to determine the cross section for production of the $\Omega^{*-}(2250)$ with decay to $\Xi^{*o}(1530)K^-$, also corrected for unseen charge modes. The result was 630 ± 180 nb.

5. DISCUSSION

Evidence for Ω^{*-} production has been reported in only one other experiment. Using a charged hyperon beam from the CERN SPS, WA42 observed a significant signal at 2251 MeV/c^2 and a further, less compelling signal at 2384 MeV/c^2, both in $\Xi^-K^-\pi^+$ systems from 116 GeV/c Ξ^-Be collisions.[2] In the same experiment no clear evidence for structure in the $\Omega^-\pi^+\pi^-$ system was seen.[7] A comparison of data between the two experiments is given in Table I below.

Table I. Summary of Ω^{*-} data.

	LASS E135	SPS WA42
Reaction	K^-p @ 11 GeV/c	Ξ^-Be @ 116 GeV/c
State 1:		
$M_\circ$ (MeV/c^2)	2253 ± 13	2251 ± 12
$\Gamma_\circ$ (MeV/c^2)	81 ± 38	48 ± 20
Events in signal	44 ± 11	78 ± 23
Decay modes	$\Xi^{*\circ}(1530)K^-$ dominant. $\Xi^-K^-\pi^+/\Xi^{*\circ}K^-$ $< 0.2(90\% c.l.)$	$\Xi^{*\circ}K^-/\Xi^-K^-\pi^+$ $= 0.7 \pm 0.2$
State 2:		
$M_\circ$ (MeV/c^2)	2474 ± 12	not observed
$\Gamma_\circ$ (MeV/c^2)	72 ± 33	"
Events in signal	52 ± 10	"
Decay modes observed	$\Omega^-\pi^+\pi^-$ >0.075	"
State 3:		
$M_\circ$ (MeV/c^2)	not observed	2384 ± 12
$\Gamma_\circ$ (MeV/c^2)	"	26 ± 23
Events in signal	"	45 ± 10
Decay modes observed	"	$\Xi^-\overline{K^{*\circ}}/\Xi^-K^-\pi^+$ $= 0.5 \pm 0.3$

In making comparisons between the two experiments, we note that in addition to considerable differences in acceptance, the very different nature of K^-p and Ξ^-Be production mechanisms forces us to conclude that no conflict exists with respect to signals observed. In particular, the $\Omega^{*-}(2470)$ observed as a five standard deviation effect in LASS, but not in WA42, could be explained as a difference in observable cross section. A similar conclusion might be made for the signal in

$\Xi^- \overline{K^{*o}}(890)$ seen by WA42 and not LASS.

Evidence for at least one state near 2250 MeV/c^2 appears to be very solid. Both E135 and WA42 observed signals with similar mass and width values, and in both cases a significant $\Xi^{*o}(1530)K^-$ decay mode was evident. However, it is somewhat speculative to equate the states seen, since:

- The two experiments differ somewhat in estimated three body $\Xi^- K^- \pi^+$ decay rates;
- Neither experiment was able to identify the J^P of states observed since both were subject to acceptance and statistical limitations imposed by K^- identification criteria;

and finally

- Several states near this mass are expected in the $\Xi^{*o}(1530)K^-$ decay mode.

Predictions for excited Ω^- states exist. Most obviously, the known Δ and Σ baryon spectra have led to the expectation of several such states. For example, pairing up the six best established Δ's with Σ states having the same spin-parities and using the Gell-Mann-Okubo equal spacing rule, leads to Ω^- baryons, at:

$$\begin{array}{ll} \sim 2000 \pm 100(\mathrm{MeV/c^2}) & (1/2^-) \\ \sim 2200 \pm 50(\mathrm{MeV/c^2}) & (7/2^+,\ 1/2^-) \\ \sim 2400 \pm 100(\mathrm{MeV/c^2}) & (1/2^+,\ 5/2^+,\ 3/2^-) \quad . \end{array}$$

A calculation using a $q-q$ interquark potential $A+Br^{0.1}$ with A and B derived from the meson spectrum has been made by J. M. Richard.[8] By including spin-spin forces, he computed, in addition to the ground state $(3/2^+)$ Ω^- at 1672 MeV/c^2, the expectation of radially excited Ω^- states at:

$$\begin{array}{ll} 2244\ (\mathrm{MeV/c^2}) & (3/2^+) \\ 2358\ (\mathrm{MeV/c^2}) & (1/2^+,\ 3/2^+,\ 5/2^+) \quad . \end{array}$$

The most detailed prediction of the Ω^- spectrum, and of the expected decay rates was made by Chao, Isgur and Karl (CIK).[9] This model included elements of QCD and confinement in describing flavor-independent $q-q$ forces in a simple harmonic oscillator potential. Parameters in the model were determined from other sectors of the baryon spectrum and decay rates. Orbitally excited states with masses above 2100 MeV/c^2 were predicted at:

2020 (MeV/c^2)	$(1/2^-,\ 3/2^-)$
2225 (MeV/c^2)	$(5/2^+)$
2265 (MeV/c^2)	$(3/2^+, 5/2^+)$.

However, no radial excitations were calculated.

It is interesting to observe that the two states at 2265 MeV/c^2 were predicted to have predominant decay to $\Xi^{*\circ}(1530)K^-$. Obviously, without measuring J^P, however, spectroscopic assignment of the signals seen in this system in both the LASS and WA42 experiments is not possible.

The $\Omega^{*-}(2470)$ has a mass above the range computed in Ref. 9. This fact alone suggests it is a radial excitation. Further evidence supporting such interpretation might be found in the large $\Omega^-\pi^+\pi^-$ decay mode observed, and the lack of any evidence for a two-body decay, for instance, to $\Xi^{*\circ}K^-$ or $\Xi^-\overline{K^{*\circ}}$. The decay branching ratio to $\Omega^-\pi\pi$ appears to be at least 7.5%. The cross section we observed, corrected for the unseen $\Omega^-\pi^\circ\pi^\circ$, was 290 nb; while the inclusive cross section for Ω^- production at this energy was 3.9 ± 0.6 μb.[6] A large decay to dipion states has been a recognized characteristic of radially excited states in both K^* and quarkonium systems. The suppression of two-body decays relative to such modes is expected, under certain circumstances, on the basis of the dynamics of radially excited quark systems.[10]

The lowest Ω^- excitations expected have masses below 1900 MeV/c^2, and have yet to be observed. Within the framework of the CIK model, they are expected to decay mostly to $\Xi^-\overline{K^\circ}$ or $\Xi^\circ K^-$. For states below 1808 MeV/c^2, decay to $\Omega^-\gamma$ would be most likely. None of these modes is easily accessible to either LASS or to WA42.

SUMMARY

Excited Ω^- states at 2250 and 2470 MeV/c^2 have been seen in LASS. The former state may also have been seen in experiment WA42 in an entirely different production reaction. Some evidence exists that $\Omega^{*-}(2470)$ is a radial excitation. This state was not seen in WA42. No evidence for $\Omega^{*-}(2380)$ reported by the WA42 collaboration has been seen in LASS data. The experimental situation is not yet completely satisfactory. In particular, the lowest Ω^- excitations have not yet been observed since statistically significant samples of events containing $\Xi\overline{K}$ and $\Omega^-\gamma$ systems (the expected decay modes) have been too difficult to accumulate. Also, more data are still required to corroborate evidence for $\Omega^{*-}(2470)$ and $\Omega^{*-}(2380)$, and to make J^P measurements necessary in making spectroscopic assignments. Nonetheless, almost 30 years after the discovery of the Ω^-, the data presented here have been able to show clearly that excited Ω^- states do indeed exist.

REFERENCES

1. D. Aston *et al.,* contributed talk given by B. Ratcliff in session P09 at the International Europhysics Conference on High Energy Physics, Bari, Italy, July 1985; see S. Cooper, Rapporteur Talk in the Proceedings of this Conference, p. 947, and SLAC–PUB–3819.

2. S. F. Biagi *et al.,* Zeits. Fur Physik, **C31** (1986) 33.

3. D. Aston *et al.,* Phys. Lett. **B194** (1987) 579.

4. D. Aston *et al.,* SLAC–REP–298 (1986).

5. J. D'Amore, Ph. D. Thesis, University of Cincinnati (1988), (unpublished).

6. D. Aston *et al.,* Phys. Rev. **D32** (1985) 2270.

7. P. Rosselet, *Proc. of the Second International Conf. on Hadron Spectroscopy,* KEK, Tsukuba, Japan, April 1987.

8. J. M. Richard, Phys. Lett. **100B** (1981) 515.

9. N. Isgur and G. Karl, Phys. Rev. **D19** (1979) 2653.

10. A. Bradley, J. Phys. **G4** (1978) 1517; E. Eichten *et al.,* Phys. Rev. **D21** (1980) 203; S. B. Gerasimov *et al.,* Z. Phys. **C13**, (1982) 43.

FIGURE CAPTIONS

Fig. 1. The LASS Spectrometer.

Fig. 2. Basic V$^-$ event topology. Solid lines indicate tracks required in the primary selection process described in the text.

Fig. 3. Distribution of the $\Lambda\pi^-$ effective mass for events selected as Ξ^- candidates as described in the text.

Fig. 4. Momentum distributions for three classes of negative charged particles produced in conjunction with Ξ^-'s. The curves are drawn to aid in distinguishing the three classes. The solid line indicates those tracks which gave no Čherenkov light; the dotted curve connects data points for the tracks which did give light. The latter data are weighted by a factor ϵ^{-1}, where ϵ is the momentum dependent Čherenkov efficiency. The dashed line shows the same data plotted instead with a weight $\epsilon^{-1}(1-\epsilon)$.

Fig. 5. Distribution of $\Xi^- K^- \pi^+$ effective masses for all 1,259 combinations. The dashed histogram contains events outside the $\Xi^{*o}(1530)$.

Fig. 6. Distribution of $\Xi^-\pi^+$ effective masses for 814 events with both a Ξ^- and a K^-. The limits used to define both $\Xi^{*o}(1530)$, and the control regions on either side are marked by arrows.

Fig. 7. Distribution of $\Xi^- K^- \pi^+$ effective masses for events having both a K^- and $\Xi^-\pi^+$ mass in the range $1510 < M_{\Xi^-\pi^+} < 1555\mathrm{MeV/c^2}$ (outer histogram); or in the control bands defined by $M_{\Xi^-\pi^+} < 1510$ or $1555 < M_{\Xi^-\pi^+} < 1600\mathrm{MeV/c^2}$ (solid dots). The open circle distribution is for events with $\Xi^-\pi^+$ mass in the former range and a negative track giving light in either C_1 or C_2. In this distribution, each event is weighted by the factor $(1-\epsilon)/\epsilon$, in which ϵ is the Čherenkov efficiency.

Fig. 8. Distribution of $\Xi^- K^- \pi^+$ effective masses for events with a $\Xi^-\pi^+$ mass in the range $1510 < M_{\Xi^-\pi^+} < 1555$ MeV/c^2, and a negative track giving light in either C_1 or C_2 with a K^- mass assignment. This sample contains no events contributing to the outer histogram in Fig. 7, but when each event is weighted by the factor $(1-\epsilon)/\epsilon$, yields the distribution with open circles in that figure.

Fig. 9. Background subtracted $\Xi^{*o}(1530)K^-$ mass distribution.

Fig. 10. The ΛK^- mass distribution for the inclusive Ω^- events; the solid histogram corresponds to those events having at least one pair of oppositely-charged primary vertex tracks consistent with a $\pi^+\pi^-$ interpretation; the dashed curve is for all events. The curve is a fit to the resolution function, determined from a Monte Carlo sample, with a linear background.

Fig. 11. (a) The inclusive $\Omega^-\pi^+\pi^-$ mass distribution for those events within ± 10 MeV/c^2 of the nominal Ω^- mass in the solid histogram of Fig. 10; for the

$\pi^{\pm}$ tracks, any available particle identification information was required to be consistent with the pion mass assignment. The dotted histogram corresponds to Čherenkov-identified π^{+}'s. The dashed histogram represents the $\Omega^{-}\pi^{\pm}\pi^{\pm}$ distribution weighted as described in the text. (b) The mass distribution obtained from the solid histogram of Fig. 11(a) when the π^{+} track is given the K^{+} mass.

Fig. 12. The ΛK^{-} effective mass from the reaction $K^{-}p \rightarrow \Lambda K^{+}K^{-}$.

Fig. 13. (a)–(c) The momentum dependence of the difference between time-of-flight calculated on the assumption of the kaon mass (t^{K}_{calc}) and the measured value: (a) for K^{-}'s from reaction (2); (b) for negative; (c) for positive primary tracks produced in association with an Ω^{-}; (d)–(f) the momentum dependence of the natural logarithm of the kaon to pion probability ratio for tracks having dE/dx information from the cylindrical PWC package surrounding the target: (d) for K^{+}'s from reaction (2); (e) for negative, and (f) for positive primary tracks produced in association with an Ω^{-}.

Fig. 14. (a) The $\Omega^{-}\pi^{+}\pi^{-}$ mass distribution corresponding to those π^{+} tracks having TOF information such that $t^{K}_{calc} \geq t_{meas}$; the dashed histogram is for those having $t^{K}_{calc} \leq t_{meas}$; (b) The $\Omega^{-}\pi^{+}\pi^{-}$ mass distribution for the "net identified π^{+}" sample described in the text.

Fig. 15. Distributions of $\pi^{+}\pi^{-}$ effective mass in three $\Omega^{-}\pi^{+}\pi^{-}$ mass ranges: (a) below; (b) in; (c) above the peak at $\sim$ 2470 MeV/c^{2}. The curves are from Monte Carlo data with purely $s-$wave dipion systems.

Fig. 16. The histogram is the solid histogram of Fig. 11(a); the curve is obtained from a fit using an S-wave Breit–Wigner line-shape plus a polynomial background (dashed curve); the resulting mass and width values are as indicated.

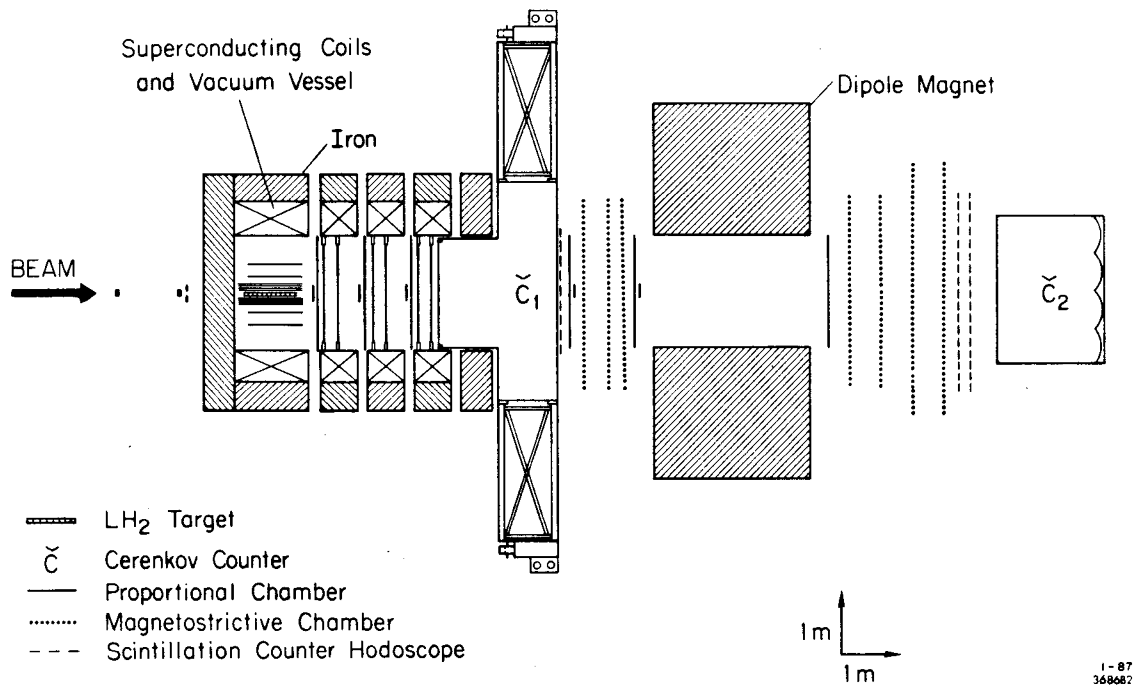
Superconducting Coils
and Vacuum Vessel
Iron
Dipole Magnet
BEAM
$\check{C}_1$
$\check{C}_2$
LH_2 Target
$\check{C}$ Cerenkov Counter
Proportional Chamber
Magnetostrictive Chamber
Scintillation Counter Hodoscope
1 m
1 m
1-87
368682

Fig. 1

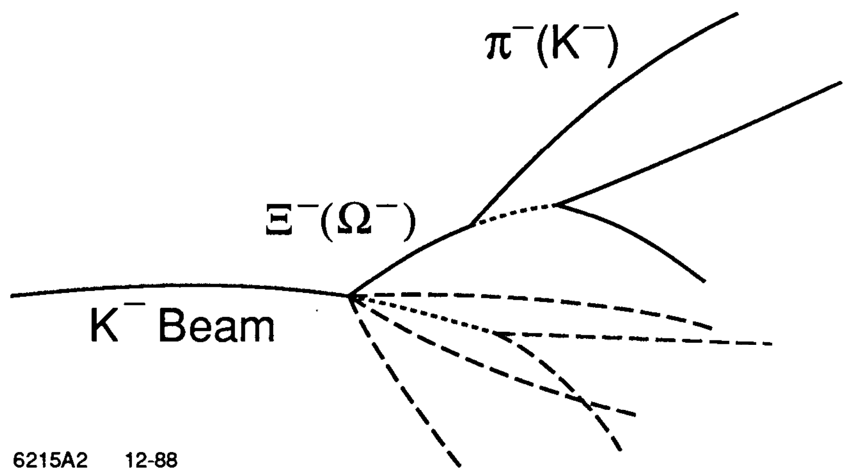

Fig. 2

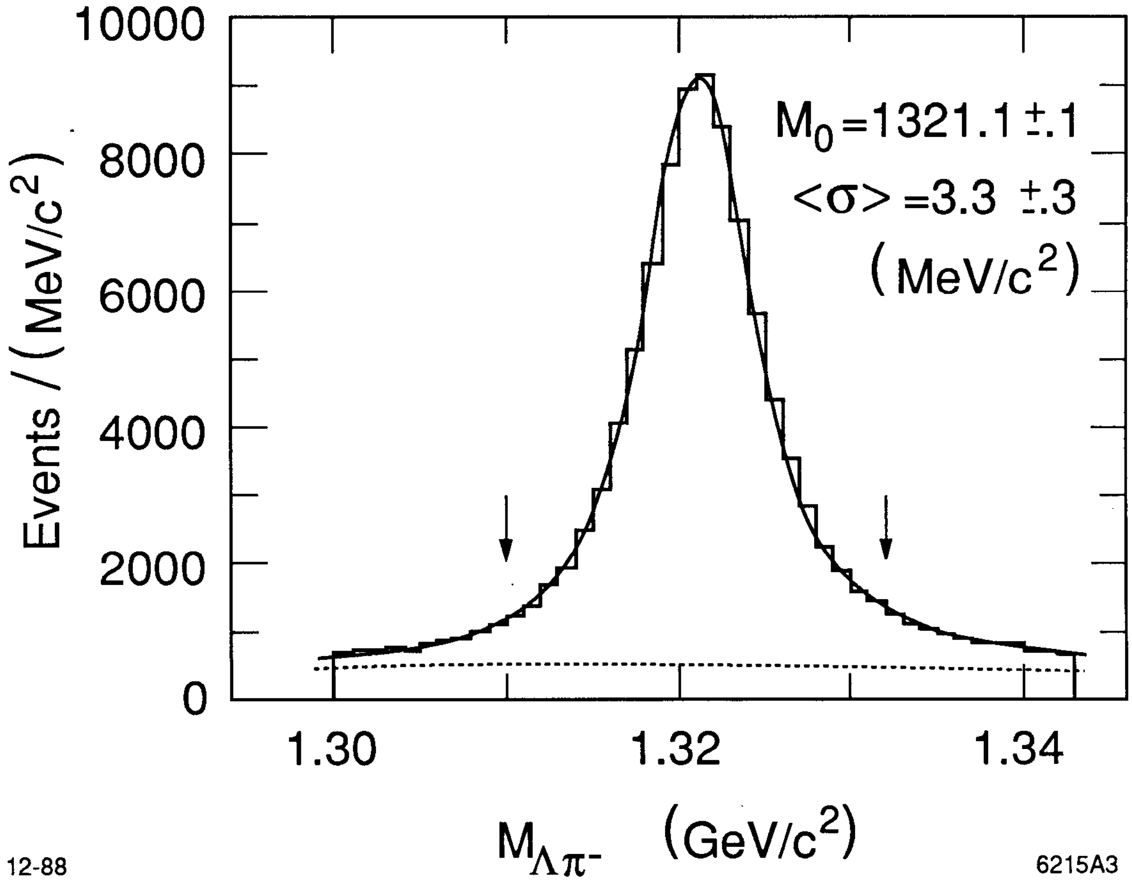

10000
8000
6000
4000
2000
0
Events / (MeV/c2)
M0 =1321.1 ±.1
<σ> =3.3 ±.3
(MeV/c2)
1.30
1.32
1.34
MΛπ- (GeV/c2)
12-88
6215A3

Fig. 3

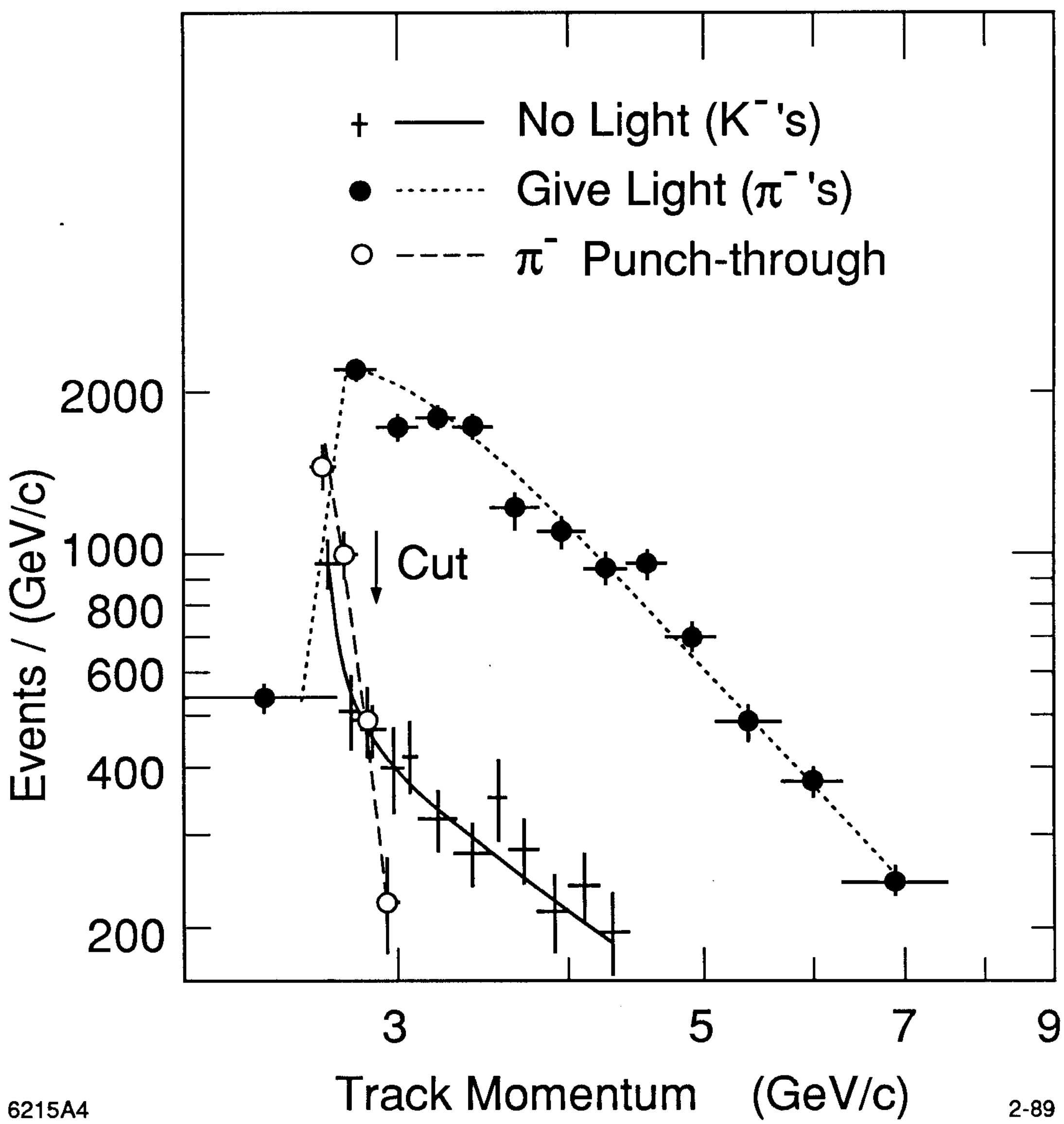

No Light (K⁻'s)
Give Light (π⁻'s)
π⁻ Punch-through
Cut
2000
1000
800
600
400
200
Events / (GeV/c)
3
5
7
9
Track Momentum (GeV/c)
6215A4
2-89

Fig. 4

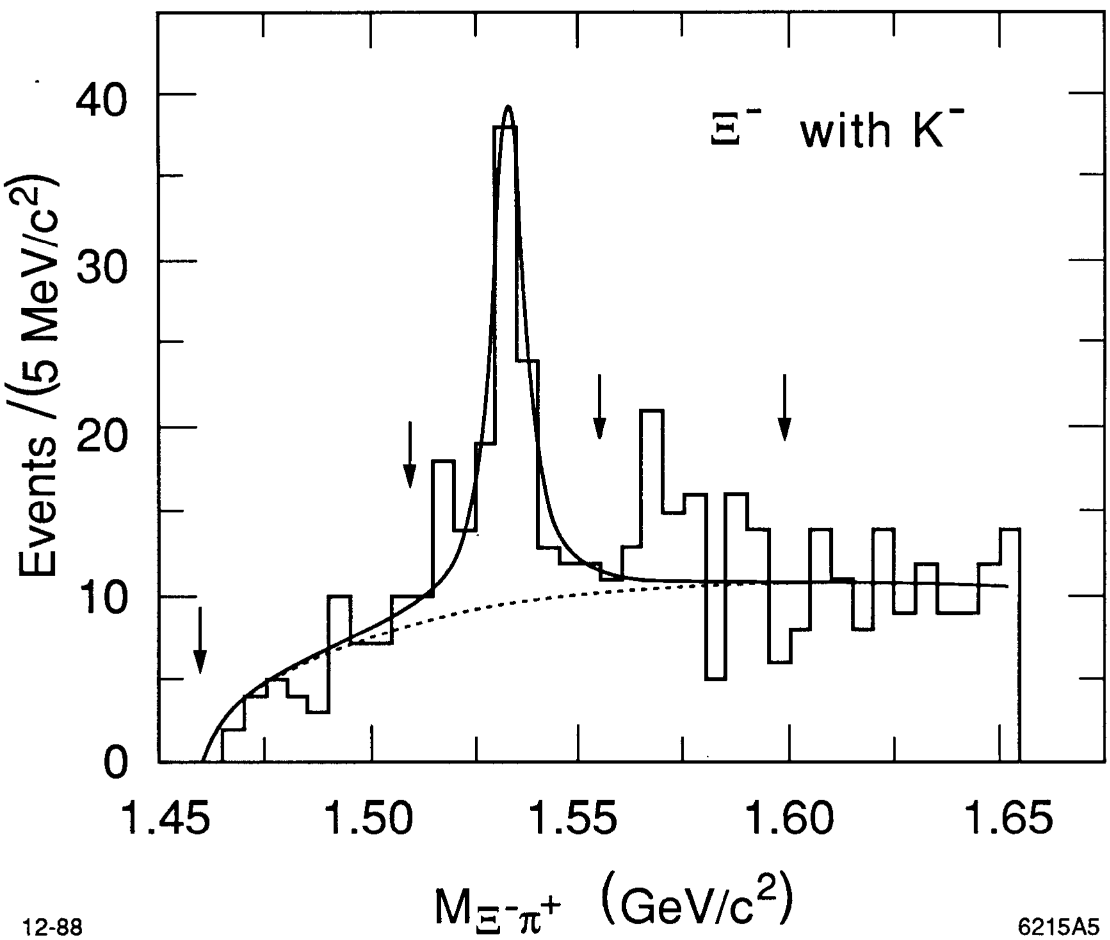

40
30
20
10
0
Events /(5 MeV/c^2)
Ξ^- with K^-
1.45
1.50
1.55
1.60
1.65
$M_{\Xi^-\pi^+}$ (GeV/c^2)
12-88
6215A5

Fig. 5

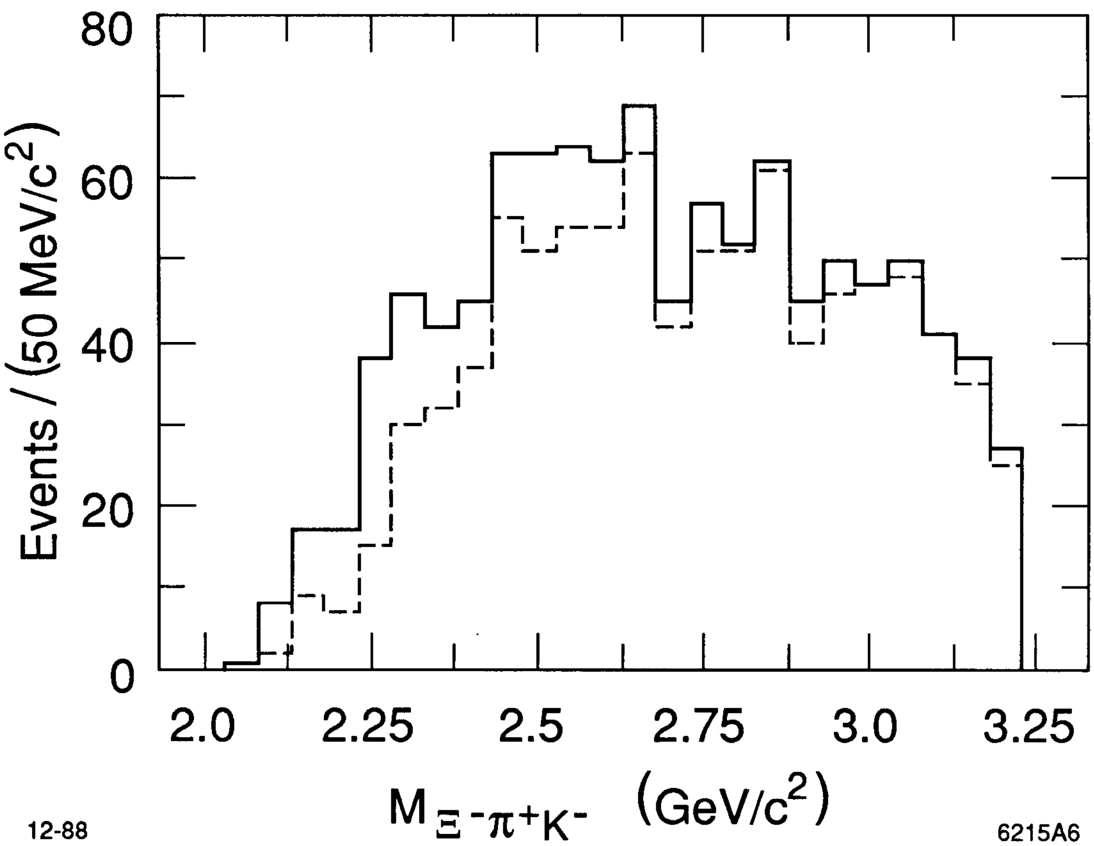

80
60
40
20
0
Events / (50 MeV/c^2)
2.0
2.25
2.5
2.75
3.0
3.25
M Ξ-π+K- (GeV/c^2)
12-88
6215A6

Fig. 6

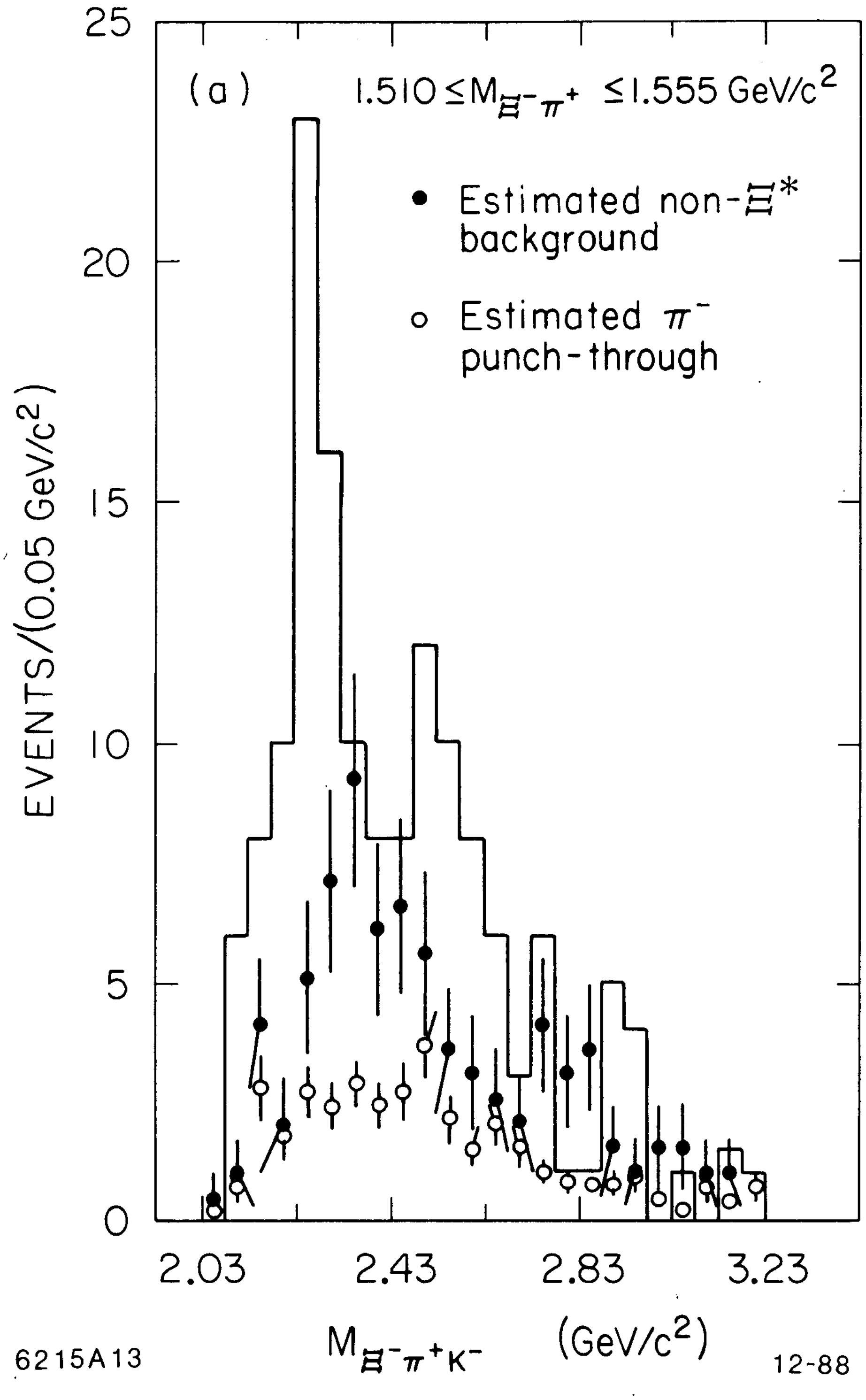
(a)
1.510 ≤ $M_{\Xi^-\pi^+}$ ≤ 1.555 GeV/c^2
Estimated non-Ξ^* background
Estimated π^- punch-through
EVENTS/(0.05 GeV/c^2)
25
20
15
10
5
0
2.03
2.43
2.83
3.23
$M_{\Xi^-\pi^+K^-}$ (GeV/c^2)
6215A13
12-88

Fig. 7

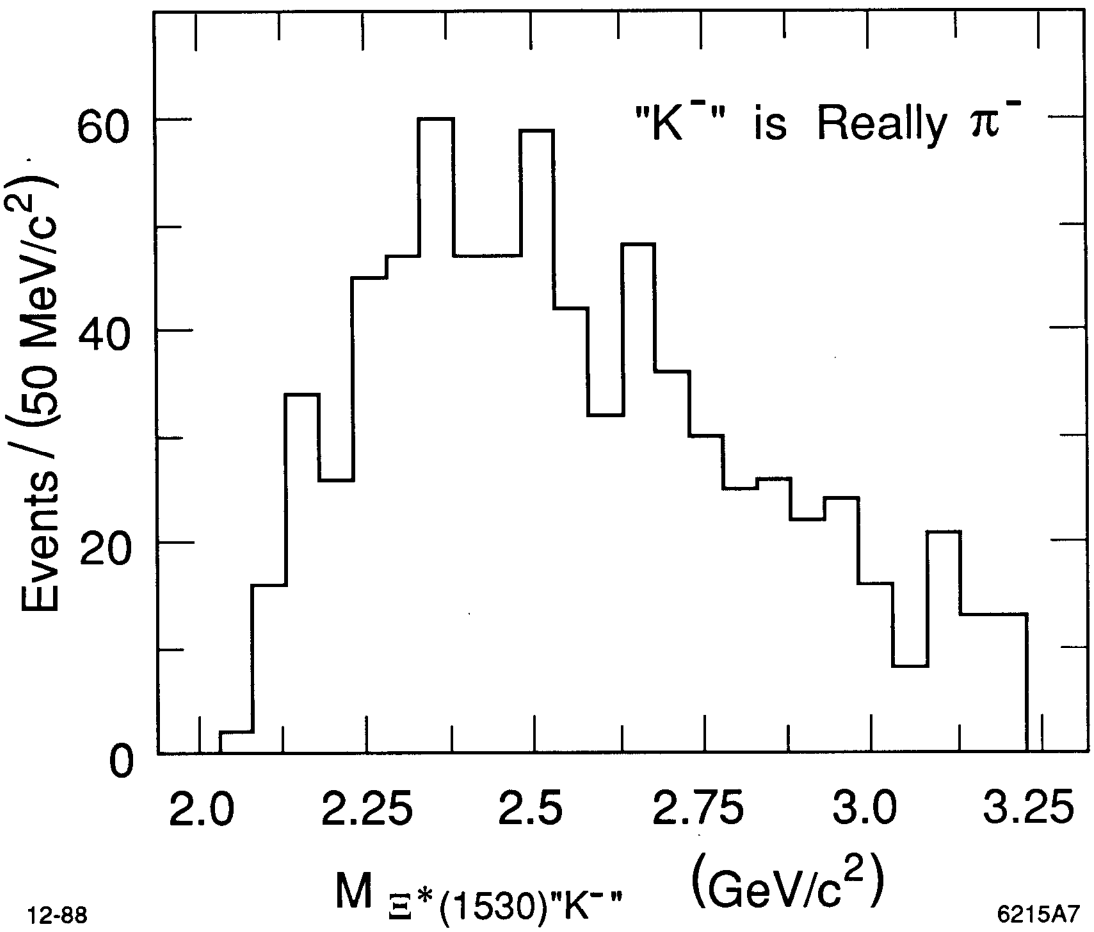

"K⁻" is Really π^-
60
40
20
0
Events / (50 MeV/c^2)
2.0
2.25
2.5
2.75
3.0
3.25
$M_{\Xi^*(1530)\text{"}K^-\text{"}}$ (GeV/c^2)
12-88
6215A7

Fig. 8

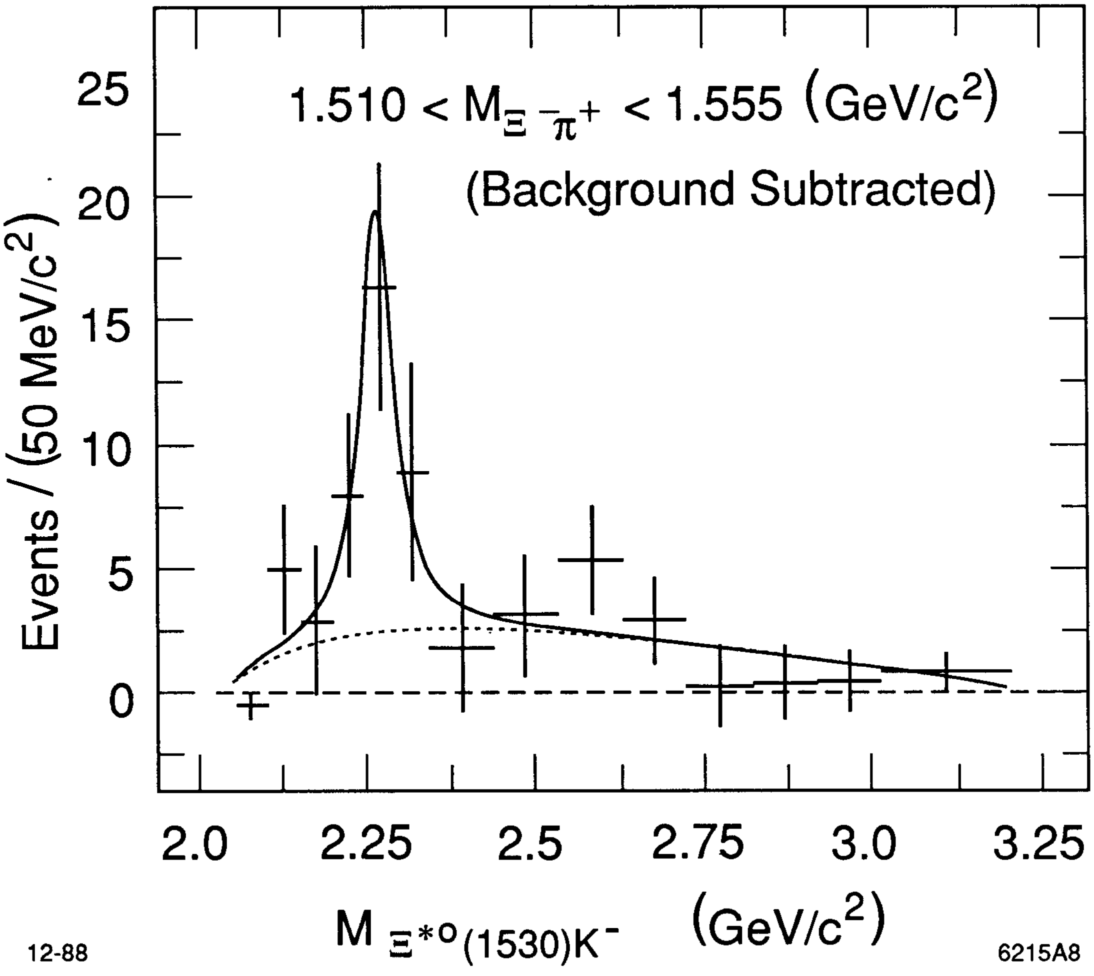

1.510 < $M_{\Xi^-\pi^+}$ < 1.555 (GeV/c²)
(Background Subtracted)
Events / (50 MeV/c²)
25
20
15
10
5
0
2.0
2.25
2.5
2.75
3.0
3.25
$M_{\Xi^{*o}(1530)K^-}$ (GeV/c²)
12-88
6215A8

Fig. 9

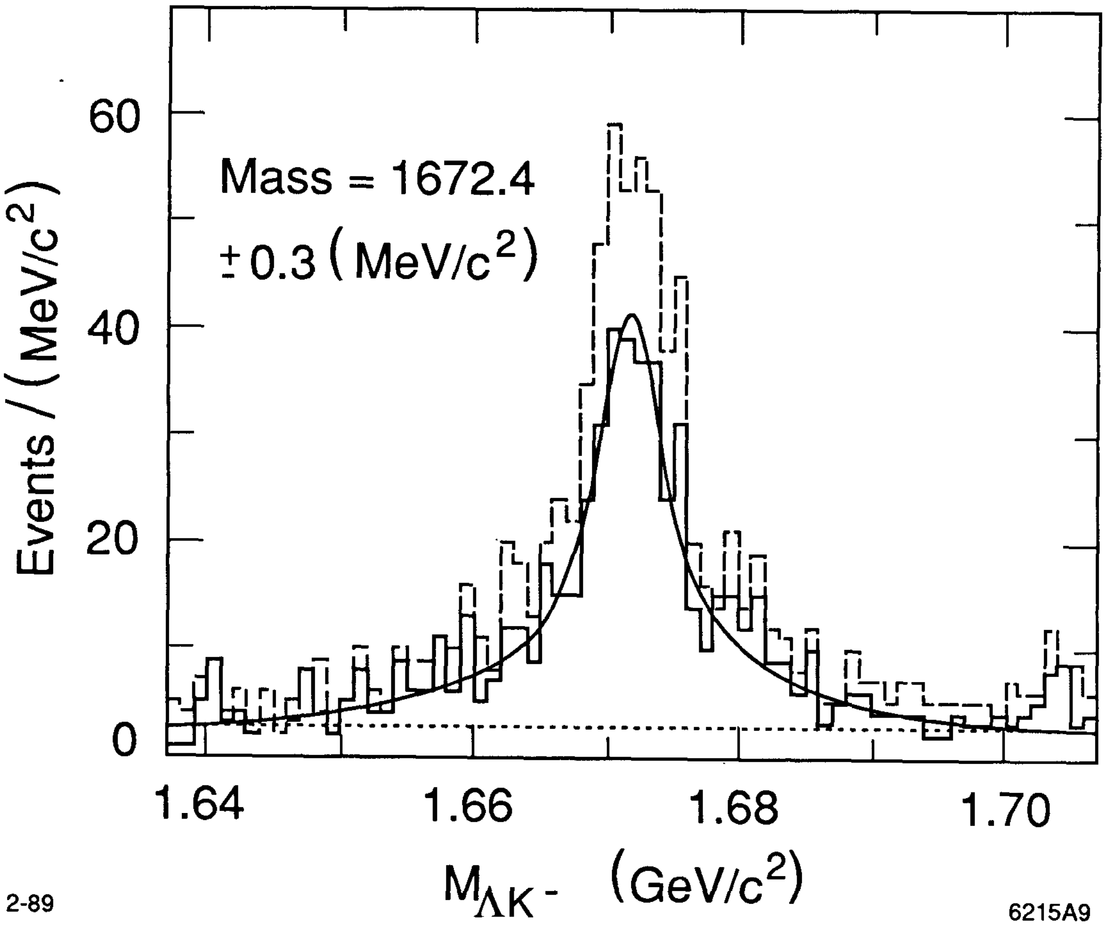

Mass = 1672.4
± 0.3 (MeV/c^2)
Events / (MeV/c^2)
0
20
40
60
1.64
1.66
1.68
1.70
$M_{\Lambda K^-}$ (GeV/c^2)
2-89
6215A9

Fig. 10

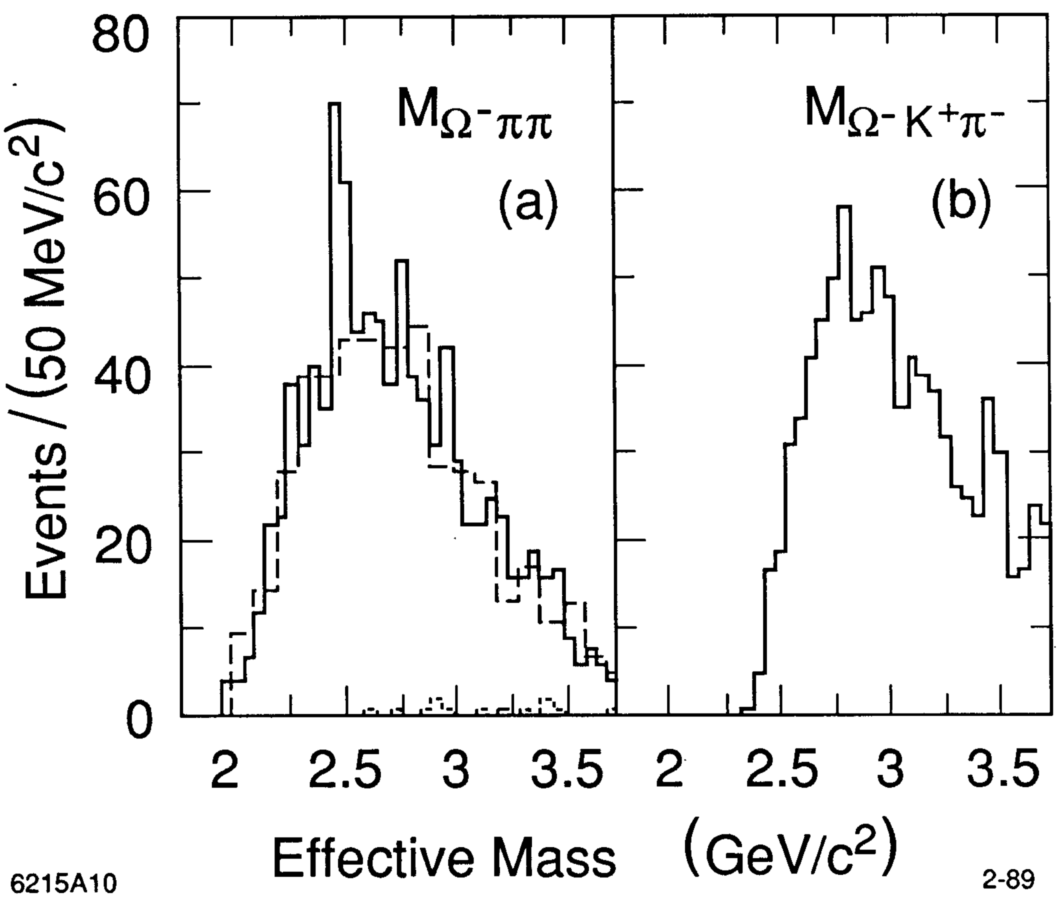
80
60
40
20
0
Events / (50 MeV/c^2)
$M_{\Omega^-\pi\pi}$
(a)
$M_{\Omega^- K^+\pi^-}$
(b)
2
2.5
3
3.5
2
2.5
3
3.5
Effective Mass (GeV/c^2)
6215A10
2-89

Fig. 11

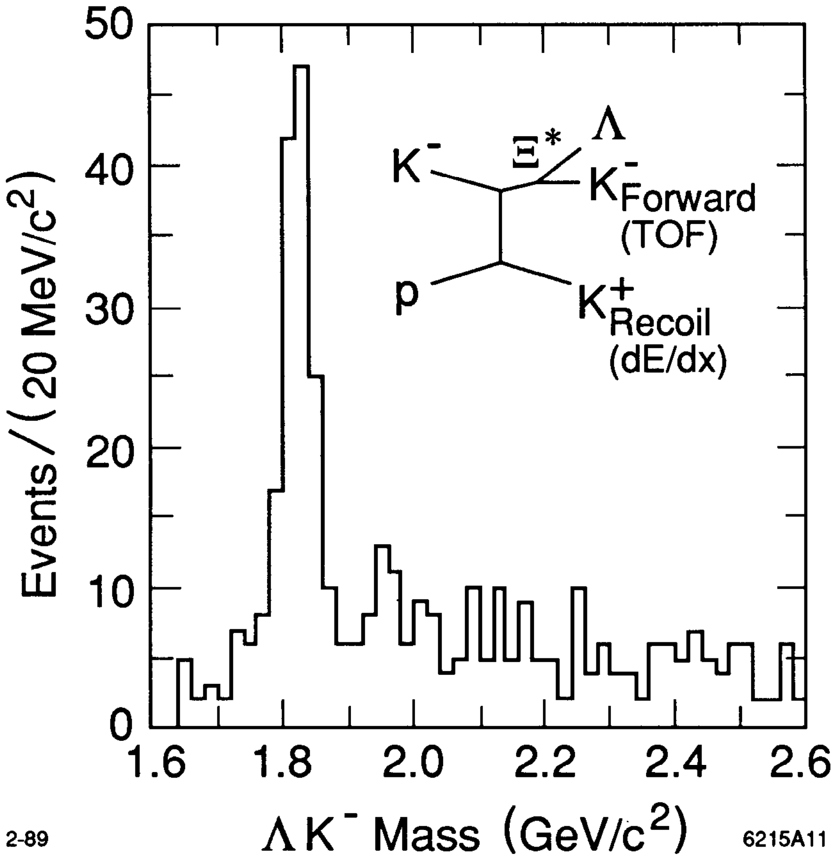
Events / (20 MeV/c^2)
ΛK$^-$ Mass (GeV/c^2)
K$^-$
p
Ξ*
Λ
K$^-_{Forward}$
(TOF)
K$^+_{Recoil}$
(dE/dx)
2-89
6215A11

Fig. 12

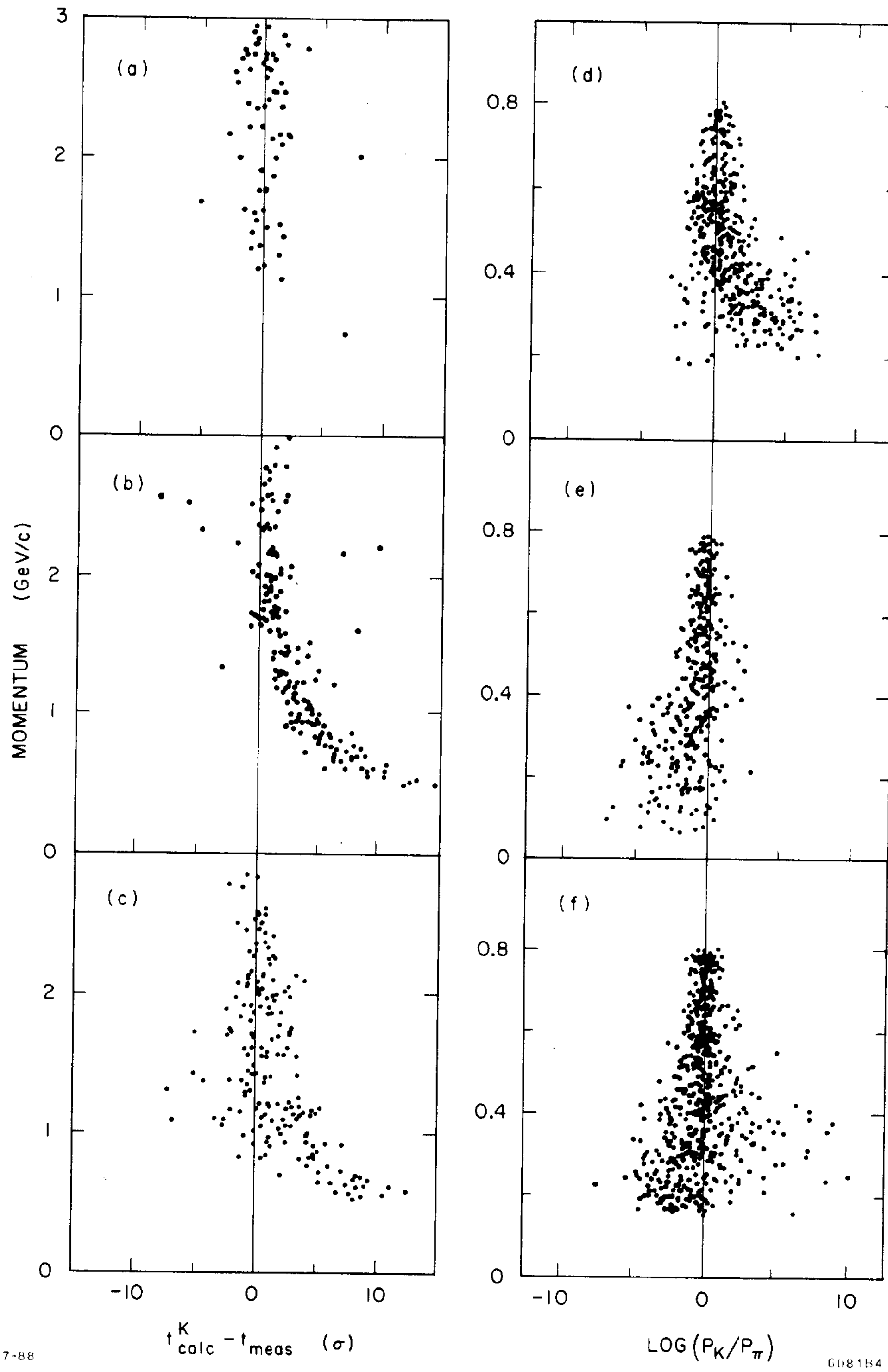
(a)
(b)
(c)
(d)
(e)
(f)
MOMENTUM (GeV/c)
$t^{K}_{calc} - t_{meas}$ (σ)
LOG (P_K/P_π)
7-88
6081B4

Fig. 13

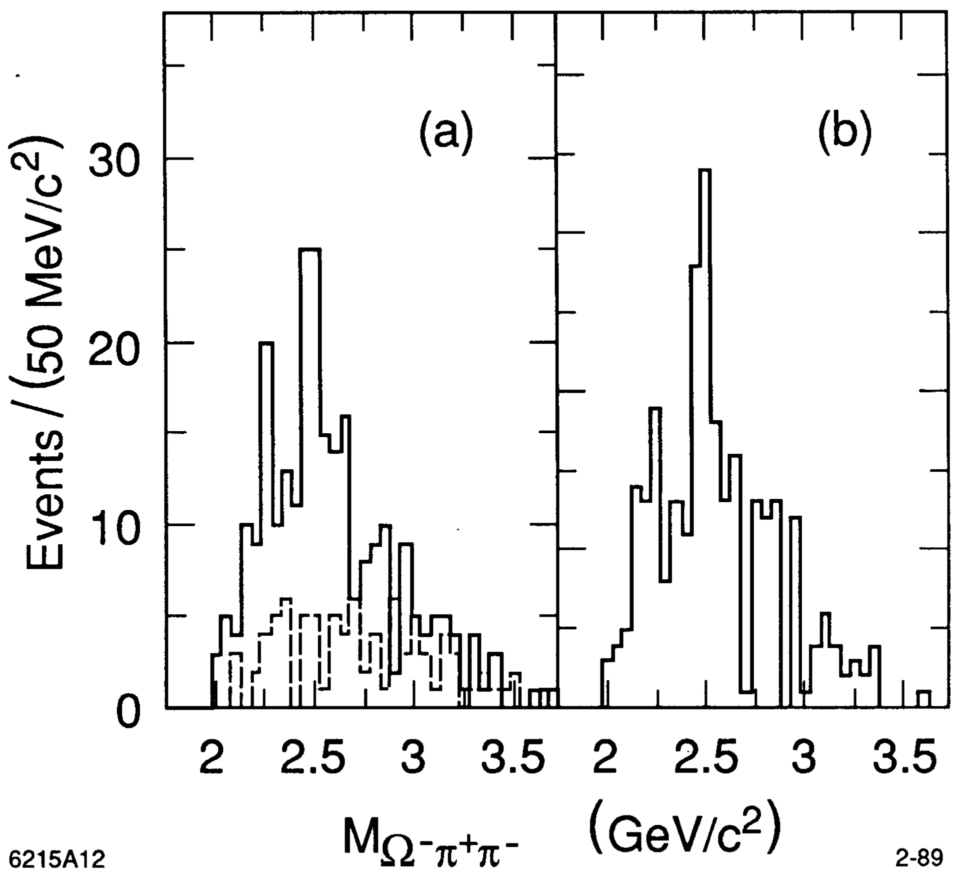

Fig. 14

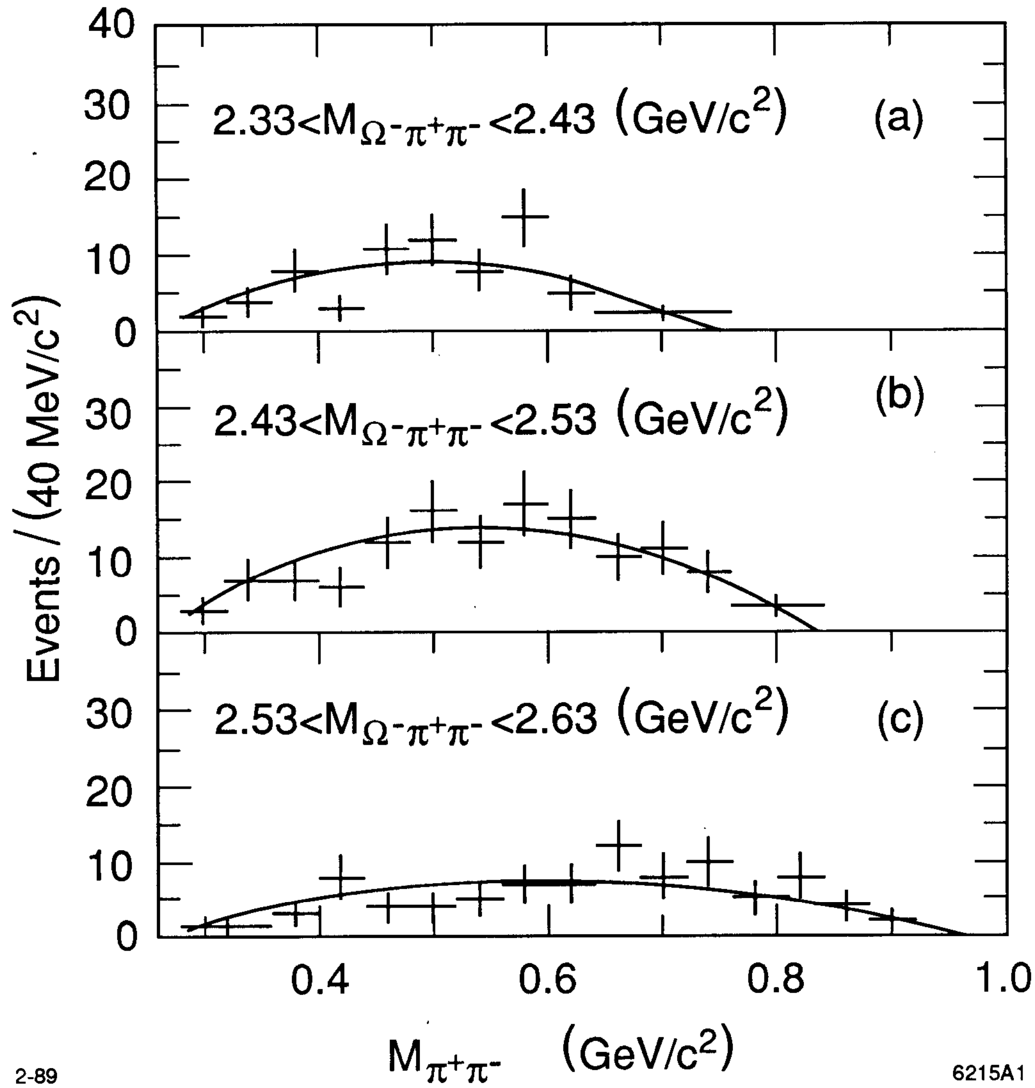

40
30
20
10
0
$2.33 < M_{\Omega^-\pi^+\pi^-} < 2.43$ (GeV/c^2)
(a)
$2.43 < M_{\Omega^-\pi^+\pi^-} < 2.53$ (GeV/c^2)
(b)
$2.53 < M_{\Omega^-\pi^+\pi^-} < 2.63$ (GeV/c^2)
(c)
Events / $(40\ MeV/c^2)$
0.4
0.6
0.8
1.0
$M_{\pi^+\pi^-}$ (GeV/c^2)
2-89
6215A1

Fig. 15

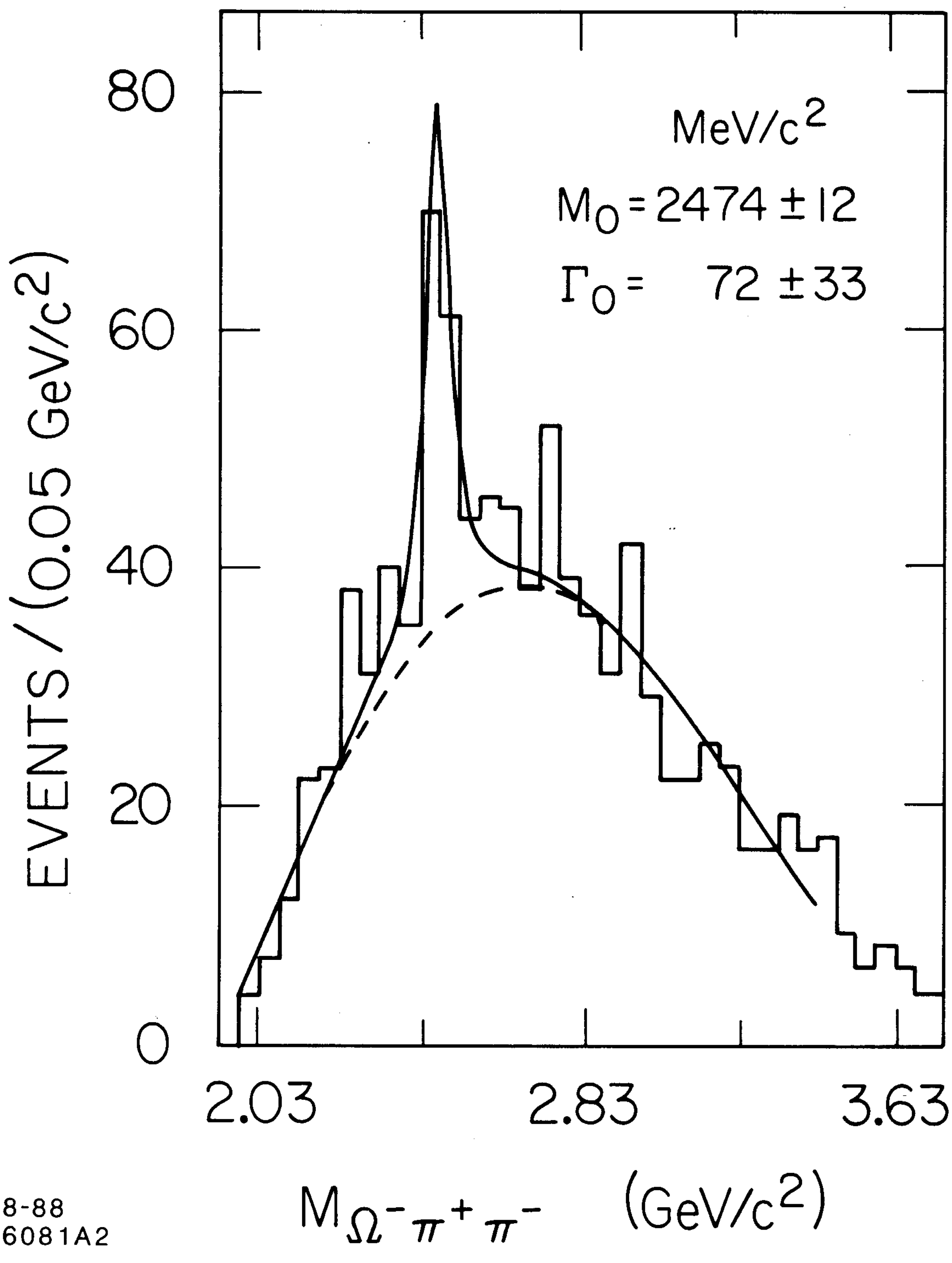

8-88
6081A2

Fig 16